The Astrophysical Journal, 774:76 (6pp), 2013 September 1 doi:10.1088/0004-637X/774/1/76

NEW *FERMI*-LAT EVENT RECONSTRUCTION REVEALS MORE HIGH-ENERGY GAMMA RAYS FROM GAMMA-RAY BURSTS

W. B. Atwood[1], L. Baldini[2], J. Bregeon[3], P. Bruel[4], A. Chekhtman[5,14], J. Cohen-Tanugi[6], A. Drlica-Wagner[7], J. Granot[8], F. Longo[9,10], N. Omodei[7], M. Pesce-Rollins[3], S. Razzaque[11], L. S. Rochester[7], C. Sgrò[3], M. Tinivella[3], T. L. Usher[7], and S. Zimmer[12,13]

[1] Santa Cruz Institute for Particle Physics, Department of Physics and Department of Astronomy and Astrophysics, University of California at Santa Cruz, Santa Cruz, CA 95064, USA
[2] Università di Pisa and Istituto Nazionale di Fisica Nucleare, Sezione di Pisa, I-56127 Pisa, Italy
[3] Istituto Nazionale di Fisica Nucleare, Sezione di Pisa, I-56127 Pisa, Italy; melissa.pesce.rollins@pi.infn.it
[4] Laboratoire Leprince-Ringuet, École polytechnique, CNRS/IN2P3, Palaiseau, France
[5] Center for Earth Observing and Space Research, College of Science, George Mason University, Fairfax, VA 22030, USA
[6] Laboratoire Univers et Particules de Montpellier, Université Montpellier 2, CNRS/IN2P3, F-34095 Montpellier, France
[7] W. W. Hansen Experimental Physics Laboratory, Kavli Institute for Particle Astrophysics and Cosmology, Department of Physics and SLAC National Accelerator Laboratory, Stanford University, Stanford, CA 94305, USA; nicola.omodei@stanford.edu
[8] Department of Natural Sciences, The Open University of Israel, 1 University Road, P.O. Box 808, Ra'anana 43537, Israel; granot@openu.ac.il
[9] Istituto Nazionale di Fisica Nucleare, Sezione di Trieste, I-34127 Trieste, Italy
[10] Dipartimento di Fisica, Università di Trieste, I-34127 Trieste, Italy
[11] Department of Physics, University of Johannesburg, Auckland Park 2006, South Africa
[12] Department of Physics, Stockholm University, AlbaNova, SE-106 91 Stockholm, Sweden
[13] The Oskar Klein Centre for Cosmoparticle Physics, AlbaNova, SE-106 91 Stockholm, Sweden
Received 2013 May 5; accepted 2013 July 5; published 2013 August 19

ABSTRACT

Based on the experience gained during the four and a half years of the mission, the *Fermi*-LAT Collaboration has undertaken a comprehensive revision of the event-level analysis going under the name of Pass 8. Although it is not yet finalized, we can test the improvements in the new event reconstruction with the special case of the prompt phase of bright gamma-ray bursts (GRBs), where the signal-to-noise ratio is large enough that loose selection cuts are sufficient to identify gamma rays associated with the source. Using the new event reconstruction, we have re-analyzed 10 GRBs previously detected by the Large Area Telescope (LAT) for which an X-ray/optical follow-up was possible and found four new gamma rays with energies greater than 10 GeV in addition to the seven previously known. Among these four is a 27.4 GeV gamma ray from GRB 080916C, which has a redshift of 4.35, thus making it the gamma ray with the highest intrinsic energy (∼147 GeV) detected from a GRB. We present here the salient aspects of the new event reconstruction and discuss the scientific implications of these new high-energy gamma rays, such as constraining extragalactic background light models, Lorentz invariance violation tests, the prompt emission mechanism, and the bulk Lorentz factor of the emitting region.

Key words: astroparticle physics – cosmology: observations – gamma rays: general – methods: data analysis

Online-only material: color figure

1. INTRODUCTION

The Large Area Telescope (LAT) on board the *Fermi Gamma-Ray Space Telescope* is a pair-conversion telescope designed to detect gamma rays above ∼20 MeV. The instrument is comprised of three subsystems acting in synergy to identify and characterize gamma-ray interactions: a silicon tracker-converter (TKR), a hodoscopic electromagnetic calorimeter (CAL), and a segmented anti-coincidence detector (ACD). By design, the TKR subsystem is divided into two distinct sections: *front* and *back*—the latter featuring six times thicker conversion foils. Since these two sections are notably different from the standpoint of the angular resolution and the contamination from misclassified cosmic rays, in the following we shall analyze separately front- and back-converting candidate gamma rays. We refer the reader to Atwood et al. (2009) for further details on the LAT.

Defining the event classes used for high-level scientific analysis is a complex process involving many different steps: the event reconstruction, the adjudication of the event energy and direction, and the final event classification. In the following, we shall refer to this process as the *event-level analysis*. The pre-launch event-level analysis was solely based on Monte Carlo simulations of the instrument performance and its particle environment, though it is worth emphasizing that significant effort was put into validating such simulations (see, e.g., Baldini et al. 2007). The event selection has been periodically updated to reflect the constantly improving knowledge of the detector and the environment in which it operates. Pass 7 (Ackermann et al. 2012a), released in 2011 August, represents the latest major iteration of this incremental process.

In parallel with the development of Pass 7, the LAT Collaboration has undertaken a coherent long-term effort to develop Pass 8, aimed at an extensive revision of the entire event-level analysis (Atwood et al. 2013). Recovering the effective area lost due to residual signals from out-of-time cosmic-ray events (*ghosts* hereafter) was the original and main motivation for this effort. As we shall see in the following, the scope of this development has substantially expanded along the way.

The full event-level analysis for Pass 8 is currently under development. Therefore, we cannot yet characterize its improvements in terms of instrument response functions. We can,

[14] Current address: Naval Research Laboratory, Washington, DC 20375, USA.

however, test the improvements in the new event reconstruction by systematically searching for events not previously recognized as gamma rays during the prompt phases of bright gamma-ray bursts (GRBs) for which the signal to noise is large enough that loose selection cuts on quantities measured to classify events are sufficient to identify gamma rays associated with the source.

In Section 2 we briefly review some aspects of the LAT event reconstruction, with emphasis on the modifications being introduced in Pass 8. In Sections 3 and 4, we discuss the analysis underlying the search for new high-energy gamma rays and the results of this search. Finally, in Section 5 we discuss the implications of these newly found high-energy gamma rays.

2. EVENT RECONSTRUCTION

A detailed description of the LAT event reconstruction is beyond the scope of this paper. In the following, we shall only give a brief description of the development being implemented in the context of Pass 8 that is relevant for the analysis presented here. We refer the reader to Atwood et al. (2013) for more details.

2.1. Tracker Reconstruction

High-energy gamma-ray interactions in the CAL tend to generate *backsplash* in the lower portion of the TKR, i.e., randomly hit strips due to secondary particles that have no relation to the trajectory of the original gamma ray. For back-converting events, and especially at large incidence angle, it is not uncommon for this backsplash to represent the vast majority of the TKR hits.

The Pass 6/Pass 7 TKR reconstruction is based on a track-by-track *combinatoric* pattern recognition—seeded by the CAL information when available. As such, it is subject to confusion in backsplash-dominated events, particularly if the initial position and direction estimates from the CAL are not accurate. These features combine to produce two main effects: (1) the loss of events where the TKR reconstruction fails to find any tracks and (2) the migration of events from the core of the point-spread function (PSF) to the tails because of poorly reconstructed tracks.

In Pass 8 we introduced a *global* approach, largely decoupled from the CAL reconstruction, which looks at the gamma-ray conversion as a pre-shower process and attempts to model this process by linking hits together into one or more tree-like structures. The individual tracks are then extracted from these structures and fitted. This new pattern recognition proved to be significantly more efficient at finding tracks and more robust in terms of pointing accuracy. Tests with Monte Carlo simulations and flight data show that the new TKR pattern recognition has the potential to provide a 15%–20% increase of the high-energy acceptance, with even larger improvement in the off-axis effective area, especially for photons converting in the lower part of the TKR.

2.2. Calorimeter Reconstruction

The Pass 6/Pass 7 CAL reconstruction treats the energy deposit in the CAL as a monolithic entity, grouping together all the crystals with greater than 4 MeV energy deposited. Residual ghost signals in the CAL away from the gamma-ray shower can result in such a large lever arm in the moments analysis used to derive the shower direction that they can introduce substantial errors in the measurement of the centroid and direction of the shower itself. Since the matching in event position and direction between the TKR and the CAL constitutes an important input to the background rejection, this is actually one of the main mechanisms for the ghost-induced loss of effective area at high energy.

In Pass 8 we introduced a clustering stage, based on a Minimum Spanning Tree algorithm, which proved to be effective in separating the genuine gamma-ray signal from the ghost one. In addition, the three-dimensional shower profile fit, which is our primary energy reconstruction method at high energy, was substantially improved. While the objective of this part of the work was to extend the energy reach of the LAT above 1 TeV the new method proved to provide an approximately 10% improvement in the energy resolution over the entire energy and inclination angle range.

Table 1
GRBs Used in This Work

GRB Name	Redshift	$\theta_{\rm LAT}$
GRB 080916C	4.35	48.°8
GRB 090323	3.57	57.°2
GRB 090328	0.74	64.°6
GRB 090510	0.90	13.°6
GRB 090902B	1.82	50.°8
GRB 090926	2.11	48.°1
GRB 091003	0.90	12.°3
GRB 091208B	1.06	55.°6
GRB 100414A	1.37	69.°0
GRB 110731A	2.83	3.°4

Notes. The 10 GRBs with measured redshift from the First *Fermi* GRB catalog (Fermi-LAT Collaboration 2013) used in this analysis. The angle between the GRB and the LAT boresight is also listed in the last column.

2.3. ACD Reconstruction

The basic purpose of the ACD reconstruction is to match tracks in the TKR and hits in the ACD to find reasons to classify an event as a charged particle. The most significant improvement in the ACD reconstruction we introduced in Pass 8 was to propagate the full covariance matrices associated with the TKR tracks to the ACD surfaces—i.e., effectively we now measure the distances between tracks and ACD hits in terms of measurement uncertainties rather than absolute lengths.

3. DATA SELECTION

Among the bursts in the First LAT GRB catalog (Fermi-LAT Collaboration 2013), we concentrate on the 10 GRBs for which an X-ray/optical follow-up (and therefore a measurement of the redshift) was obtained (see Table 1 for a listing of the GRBs used). The typical localization error for these bursts is negligible compared with the event-by-event direction accuracy of the LAT and, for all practical purposes, we can consider the localizations measured in the optical or X-ray afterglows as the true source positions when defining the region of interest (ROI). We further refine our sample by considering only energies greater than 10 GeV, where the width of the core of the LAT PSF is close to its asymptotic high-energy limit. It is important to stress here that the analysis described in Fermi-LAT Collaboration (2013) was done using the Pass 6 version of the gamma-ray data (and the associated `P6_V3_TRANSIENT` IRFs), rather than the reprocessed Pass 7 data made available in 2011 August. However, the event reconstruction between Pass 6 and Pass 7 remained essentially unchanged and therefore this is largely irrelevant for the purpose of this paper.

Table 2
Basic Properties of the 11 Gamma Rays Relevant for This Work

Run ID–Event ID	$t - T_0$ (s)	Type	Energy (GeV)		Angle to Source (°)		$p_{\rm all}$	Photon Class
			Pass 6	Pass 8	Pass 6	Pass 8		Pass 6
GRB 080916C ($\theta_{\rm LAT} = 48.^\circ8$, $z = 4.3$)								
243215785–2033380	16.545	Back	13.2	12.4	0.09	0.11	1.000	Diffuse
243215785–2075096⋆	40.509	Back	...	27.4	...	0.07	1.000	...
GRB 090510 ($\theta_{\rm LAT} = 13.^\circ6$, $z = 0.9$)								
263605997–3472705	0.828	Front	31.3	29.9	0.09	0.08	0.999	Transient
GRB 090902B ($\theta_{\rm LAT} = 50.^\circ8$, $z = 1.8$)								
273579835–4719473	11.671	Front	11.2	11.9	0.21	0.07	0.999	Transient
273579835–4724519⋆	14.166	Back	14.2	14.2	2.61	0.11	0.980	...
273579835–4748164⋆	26.168	Back	...	18.1	...	0.11	0.999	...
273579835–4778868	42.374	Front	8.9	12.7	0.03	0.04	0.999	Diffuse
273579835–4784978	45.608	Front	12.5	15.4	0.07	0.10	0.995	Diffuse
273579835–4852498	81.746	Back	33.4	39.9	0.78	1.77	0.998	Transient
GRB 090926 ($\theta_{\rm LAT} = 48.^\circ1$, $z = 2.1$)								
275631595–173595	24.835	Front	19.6	19.5	0.05	0.09	0.999	Diffuse
GRB 100414A ($\theta_{\rm LAT} = 69.^\circ0$, $z = 1.4$)								
292903615–2268542⋆	33.365	Front	29.8	29.7	7.64	0.16	0.999	...

Notes. In the first column are the run ID and event ID, followed by the arrival time, the conversion type, the reconstructed energy provided by Pass 6 and Pass 8, the reconstructed angle to the GRB provided by Pass 6 and Pass 8, the preliminary Pass 8 signal probability, and the Pass 6 event class for the photons from the First LAT GRB catalog (Fermi-LAT Collaboration 2013). For each GRB, $\theta_{\rm LAT}$ indicates the angle between the GRB and the LAT boresight and z is the redshift from Fermi-LAT Collaboration (2013). The four gamma-ray candidates recovered owing to the reconstruction improvements provided by Pass 8 are indicated by the ⋆ symbol in the first column. The Pass 8 angle to source for event 4852498 of GRB 090902B falls marginally outside our ROI. This is addressed in Section 3.

For each GRB we reprocessed all the available data within 90 s from the trigger time using the Pass 8 event reconstruction available at the time of writing. We select gamma-ray candidates by requiring that the reconstruction finds at least one track and that this track extrapolates to more than four radiation lengths of active material in the CAL (this helps avoiding poorly reconstructed events). In addition, we use the ACD to remove *likely* charged-particle events by requiring that the track-tile association most likely to veto the event is incompatible with being generated by a minimum ionizing particle. Note that the event selection used here does not include any requirement on the quality of the direction/energy reconstruction.

The choice of the ROI is dictated by the need to minimize the amount of solid angle over which we integrate the background of residual (misclassified) cosmic rays while at the same time retaining a reasonable efficiency for well-reconstructed gamma rays. For each GRB we used a circular ROI around the nominal source position with a radius of $0.^\circ6$ for front-converting and $1.^\circ2$ for back-converting events. It is worth noting that, while these are comparable with the PSF 95% containment radii for the cleanest Pass 6/Pass 7 event classes, based on Monte Carlo simulations we estimate that the actual containment level for the back-converting events passing our loose selection cuts is only about 80%, so that the ROI cut has a significant impact on the event topology of our sample (i.e., it plays a role in selecting well-reconstructed events).

The expected rate of background events passing these basic selection criteria can be estimated from the flight data by sideband subtraction (Ackermann et al. 2012a) using an annulus around the source position and rescaling the number of counts to the solid angle subtended by the original ROI. As the level of charged-particle background varies across the *Fermi* orbit, the results are slightly different for each individual GRB, but on average we expect ∼0.1 cosmic-ray events passing our basic selection cuts within each of the 90 s time windows.

4. RESULTS

The First LAT GRB catalog includes 7 candidate gamma rays with energies greater than 10 GeV associated with the 10 GRBs considered here; in the reprocessed version of the data we find four additional (previously misreconstructed) events passing our selection criteria. In Table 2, we summarize the basic properties of the four new gamma rays together with the seven previously known ones. All of the seven aforementioned gamma-ray candidates pass our loose selection cuts (and their topologies are highly gamma-ray-like). However, one of them (a ∼33 GeV event from GRB 090902B) is reconstructed as being marginally outside our ROI. While this is not entirely surprising (the quality of the direction reconstruction for this particular event is fairly poor both in the Pass 6 and in the Pass 8 versions of the event-level analysis), assessing the actual probability for this event to be associated with the GRB in the context of any of the actual Pass 8 event classes will only be possible once the definitions of the classes are frozen and the corresponding response functions defined.

It is interesting to note how the mechanisms through which these events are recovered tie to the problematic aspects of the LAT event reconstruction outlined in Section 2: two of them had no tracks in Pass 6, one was significantly mistracked (to more than 7° off the source), and the last one was compromised by a ghost cluster in the CAL. We would like to stress here that the Pass 8 event reconstruction is in its final phase; therefore, we are confident that the basic topological properties of these four new photons will not vary significantly and that no additional photons will be found in the same 90 s interval explored in this work.

Table 3
Spectral Analysis Results

	GRB 080916C	GRB 090902B		GRB 100414A
N_{obs}: number of Pass 6 events with energy > new Pass 8 event	0	1		0
Best-fit value of the gamma-ray index	2.1 ± 0.09	1.96 ± 0.07		2.1 ± 0.4
Expected number of events (N_{exp})	0.5	3.3	2.5	0.1
Probability of observing N_{obs} events	0.60	0.13	0.21	0.88
Probability of observing $>N_{obs}$ events	0.40	0.63*	0.71	0.12

Notes. Output from the spectral analysis for the three GRBs from which we recover the four new gamma rays. The best-fit value of the gamma-ray index is taken from Fermi-LAT Collaboration (2013). The value with the "*" is the probability of observing two additional events and refers to event 4724519 from GRB 090902B.

Table 2 shows how the preliminary Pass 8 event selection described in Atwood et al. (2013) assigns a fairly high value for the measure of gamma-ray probability p_{all} to all the 11 gamma-ray candidates considered here. While this is an uncalibrated quantity with no *direct* physical meaning (and it might very well change in future iterations of the Pass 8 event-level analysis), we find that the fraction of background events with such a high value of p_{all} is of the order of 10^{-3}. This is effectively a multiplicative factor for the ~0.1 Hz rate of background events quoted in Section 3.

Finally, we note that most of the events in the table have angular distances to the nominal source position much smaller than the radius of our ROI. Under the reasonable assumption that the background is approximately isotropic in our $\sim 1^\circ$ circle, we would expect background events to be preferentially near the edge of the ROI (just because it subtends a larger solid angle).

We estimated the increase in effective area over the Pass 6 `TRANSIENT` class expected for our selection[15] by means of a gamma-ray Monte Carlo simulation similar to those that we routinely use for generating effective area tables. Between 10 and 30 GeV this improvement is of the order of ~10% at a 50° off-axis angle and reaches ~50% at 70°. Note that the choice of off-axis angles corresponds to those of the GRBs from which we recovered the four new gamma rays. Though the small statistics in our GRB event sample does not allow a validation of the increase in effective area, these factors are consistent with our findings. We also stress that the factors refer to the particular selection used in this analysis and do not represent the actual performance of any of the still-forthcoming Pass 8 event classes.

4.1. Spectral Analysis

As stated in Section 1, a final Pass 8 event-level analysis is not yet available and therefore we cannot perform a spectral analysis. We can, however, estimate the probability of detecting these high-energy gamma rays, given the spectral properties inferred from Pass 6 analysis. Using `gtobssim`, we simulated 90 s observations of a very bright source located at the position of each of the three GRBs with new candidate gamma rays, using the best-fitted values (from Fermi-LAT Collaboration 2013) for the index of the power-law spectrum. We normalized the output of the simulation to the observed number of Pass 6 `TRANSIENT` counts above 100 MeV in an ROI of 5° in order to estimate the expected number of events, N_{exp}, above the energy of the new Pass 8 gamma ray. Finally, we use the Poisson distribution to compute the probability of observing exactly N_{obs} events when the number of expected events is N_{exp}. In addition, we calculate the probabilities of observing at least one additional gamma ray—or two additional gamma rays for GRB 090902B—with an energy equal to or greater than those recovered with Pass 8. Results are reported in Table 3.

We have studied the potential impacts that spectral evolution during the considered time interval (90 s) may have on the resulting probabilities $P(N_{exp}, N_{obs})$ by repeating the Monte Carlo simulation with a varying index for the spectral distribution of gamma rays. We find that the associated variation in the probability in the worst case[16] is of the order of 10%–15%. The calculated probabilities suggest that the additional gamma rays are statistically consistent with the shape and intensity of the spectra derived using Pass 6 data.

5. DISCUSSION

Our most interesting finding is the 27.4 GeV gamma ray from GRB 080916C that was detected 40.5 s after the burst onset. At a redshift of $z \approx 4.35$ the measured energy corresponds to an energy of ≈147 GeV in the GRB cosmological rest frame. This is the highest intrinsic energy measured so far for a gamma ray from a GRB.

The high energy of the new gamma ray from GRB 080916C is very constraining for a possible origin from synchrotron radiation. A reasonable assumption for the acceleration time of the radiating electron, that it is at least the time it takes to complete one Larmor gyration[17], would imply a minimum

[15] We included the effect of the ROI in our estimate by requiring, in addition to the preliminary Pass 8 event selection that we applied, that the angle between the true and reconstructed gamma-ray direction is smaller than the radius of the ROI itself.

[16] GRB 080916C (Abdo et al. 2009c) is the GRB in our sample that shows the largest spectral variation, with a gamma-ray index varying from 2.3 to 2.1 with an error of 0.09.

[17] This assumption implies a maximum electron Lorentz factor of $\gamma_{max} = \sqrt{3e/\sigma_T B'}$, where B' is the comoving (measured in the rest frame of the emitting plasma) magnetic field. The corresponding comoving typical synchrotron gamma ray energy averaged over an isotropic pitch-angle distribution is $E'_{syn,max} = 3heB'\gamma^2_{max}/(16 m_e c) = (27/64) m_e c^2/\alpha$, where $\alpha = e^2/\hbar c \approx 1/137$ is the fine structure constant. The corresponding observed energy is $E_{syn,max} = E'_{syn,max}\Gamma/(1+z) \approx 29.5(1+z)^{-1}(\Gamma/1000)$ GeV. Therefore, a synchrotron origin for this gamma ray would imply $E_{obs} \lesssim E_{syn,max}$ or $\Gamma \gtrsim 2030[(1+z)/3](E_{obs}/20\,\mathrm{GeV})$. The peak of the electron synchrotron spectral emissivity is 0.29 times the value for $E_{syn,max}$ used above, and using it would increase the limit correspondingly (by a factor of 1/0.29) to $\Gamma \gtrsim 7000[(1+z)/3](E_{obs}/20\,\mathrm{GeV})$. Allowing the acceleration time to be as small as the time it takes to deflect the electron by one radian (which is quite extreme) lowers the limit by a factor of 2π, to $\Gamma \gtrsim 323[(1+z)/3](E_{obs}/20\,\mathrm{GeV})$. Combining such a short acceleration time with the factor of 0.29 mentioned above leads to $\Gamma \gtrsim 1110[(1+z)/3](E_{obs}/20\,\mathrm{GeV})$. Recently, Kumar et al. (2012) have proposed a way to lower this limit by assuming two zones with significantly different magnetic field strength, where in the lower-field region electrons can be accelerated to high Lorentz factors, and then radiate energetic synchrotron gamma rays after crossing to the high-field region. This could in principle accommodate the production of ≳100 GeV gamma rays with significantly lower bulk Lorentz factors.

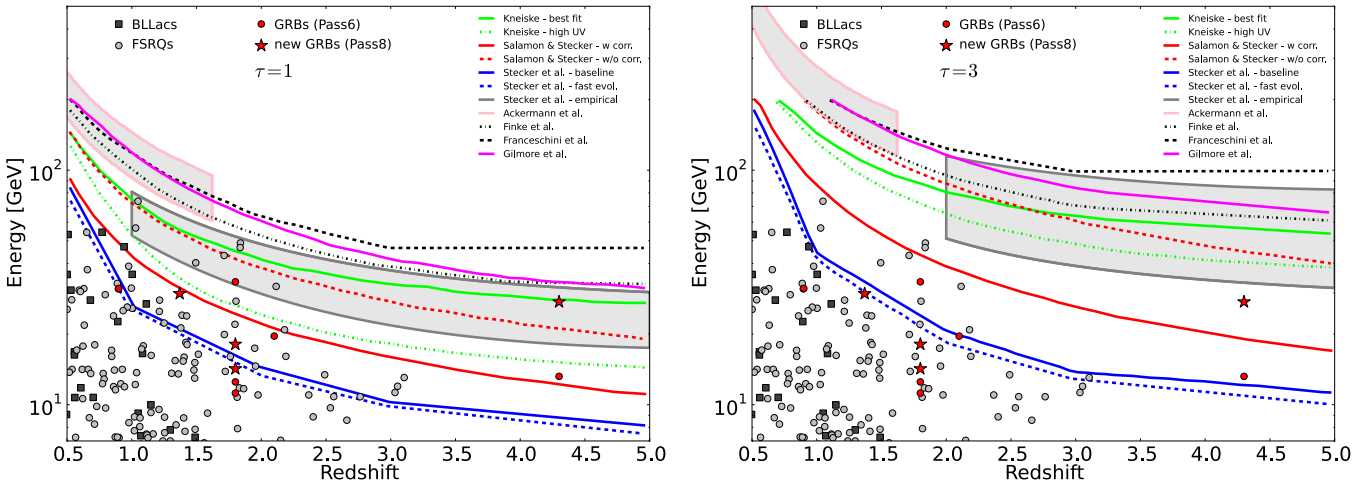

Figure 1. Highest energy gamma rays from blazars (Abdo et al. 2010), and GRBs (Fermi-LAT Collaboration 2013) seen by the LAT. Predictions of optical depth due to pair production, $\tau_{\gamma\gamma} = 1$ (left panel) and $\tau_{\gamma\gamma} = 3$ (right panel) from various EBL models are indicated by lines. The shaded area outlined in gray is the prediction from Stecker et al. (2012) and the shaded area outlined in pink is the best-fit value (1σ) measured by Ackermann et al. (2012b). Gamma rays above model predictions in this figure traverse an EBL medium with a high gamma-ray opacity. The four new gamma rays presented in this work are represented by the red stars.

(A color version of this figure is available in the online journal.)

bulk Lorentz factor of the emitting region larger than 5000. Similarly, the 29.7 GeV gamma ray from GRB 100414A at $z = 1.37$ would require $\Gamma \gtrsim 2300$ for a synchrotron origin. For GRB 090902B (Abdo et al. 2009a) at $z = 1.822$, the two new gamma rays are less constraining than the 33.4 GeV gamma ray detected 82 s after the burst onset with Pass 6, after the end of the prompt emission, which implies $\Gamma \gtrsim 3200$ (making a synchrotron origin unlikely for the 33.4 GeV gamma ray due to its later arrival time).

Given the arrival time of 40.5 s after the burst onset of the 27.4 GeV gamma ray from GRB 080916C, during interval d defined in (Abdo et al. 2009c), the lower limit on Γ due to intrinsic opacity to pair production is increased by only 15% compared to the limit from the 13 GeV gamma ray observed in the same time interval, of $\Gamma_{\rm min} \approx 600$ for a simple one-zone model, or ~3 times lower than this for a more realistic self-consistent time-dependent model (Granot et al. 2008; Hascoet et al. 2012).

Due to its later arrival time, the constraints that the new gamma ray from GRB 080916C provides on linear ($n = 1$) Lorentz invariance violation (LIV) are slightly weaker (by 15%) than the previously highest energy gamma ray from the same GRB (of energy ≈13.2 GeV detected at $t = 16.5$ s after the GRB trigger time, which implies[18] $\xi_1 = M_{\rm QG,1}/M_{\rm Planck} > 0.11$, Abdo et al. 2009c). For a quadratic leading LIV term ($n = 2$) it does slightly better with $M_{\rm QG,2} > 1.13 \times 10^{10}$ GeV/c^2, which is only ≈2.6 times below the best limit from GRB 090510 (Abdo et al. 2009b). The limits from the other new gamma rays are not as constraining.

A very interesting implication arises for the extragalactic background light (EBL) from the fact that a 27.4 GeV gamma ray has reached us from a fairly high redshift of $z \approx 4.35$, and was not attenuated (through pair production, $\gamma\gamma \rightarrow e^+e^-$) by the EBL. In particular, it is useful to compare the constraints that it provides to those from previously detected gamma rays from GRBs (Fermi-LAT Collaboration 2013) and active galactic nuclei (AGNs; Abdo et al. 2010), as illustrated in Figure 1. It is the most constraining gamma ray so far from a GRB (see Figures 3 and 5 in Abdo et al. (2010); note in particular that Figure 5 also applies to the newly found 27.4 GeV from GRB 080916C). Moreover, it is in fact comparable to or even slightly more constraining than the *Fermi*-LAT gamma rays from AGNs (for most EBL models[19] especially for $\tau = 3$ as shown in Figure 1).

In conclusion, the improvements in event reconstruction implemented in Pass 8 promise to yield scientific gains, as illustrated in this work.

The *Fermi*-LAT Collaboration acknowledges generous ongoing support from a number of agencies and institutes that have supported both the development and the operation of the LAT as well as scientific data analysis. These include the National Aeronautics and Space Administration and the Department of Energy in the United States; the Commissariat à l'Energie Atomique and the Centre National de la Recherche ScientifiqueInstitut National de Physique Nucléaire et de Physique des Particules in France; the Agenzia Spaziale Italiana and the Istituto Nazionale di Fisica Nucleare in Italy; the Ministry of Education, Culture, Sports, Science and Technology (MEXT), the High Energy Accelerator Research Organization (KEK), and the Japan Aerospace Exploration Agency (JAXA) in Japan; and the K. A. Wallenberg Foundation, the Swedish Research Council, and the Swedish National Space Board in Sweden.

Additional support for science analysis during the operations phase is gratefully acknowledged from the Istituto Nazionale di Astrofisica in Italy and the Centre National d'Études Spatiales in France.

REFERENCES

Abdo, A. A., Ackermann, M., Ajello, M., et al. 2009a, ApJL, 706, L138
Abdo, A. A., Ackermann, M., Ajello, M., et al. 2009b, Natur, 462, 331
Abdo, A. A., Ackermann, M., Ajello, M., et al. 2010, ApJ, 723, 1082

[18] The limits we quote conservatively use the lowest values within the 1σ confidence intervals for the gamma-ray energy (and the GRB redshift when relevant).

[19] A description of the different models is beyond the scope of this work; we refer the reader to the original works on the various EBL models (e.g., Salamon & Stecker 1998; Stecker et al. 2006, 2012; Kneiske et al. 2002, 2004; Primack et al. 2005; Gilmore et al. 2009; Franceschini et al. 2008; Razzaque et al. 2009; Finke et al. 2010). See also Paper I (Gilmore 2012) and Paper II (Domínguez et al. 2013) for further implications on the EBL.

Abdo, A. A., Ackermann, M., Arimoto, M., et al. 2009c, Sci, 323, 1688
Ackermann, M., Ajello, M., Albert, A., et al. 2012a, ApJS, 203, 4
Ackermann, M., Ajello, M., Allafort, A., et al. 2012b, Sci, 338, 1190
Atwood, W., Albert, A., Baldini, L., et al. 2013, arXiv:1303.3514
Atwood, W. B., Abdo, A. A., Ackermann, M., et al. 2009, ApJ, 697, 1071
Baldini, L., Barbiellini, G., Bellazzini, R., et al. 2007, in AIP Conf. Proc. 921, The First GLAST Symposium, ed. S. Ritz, P. Michelson, & C. A. Meegan (Melville, NY: AIP), 190
Domínguez, A., Finke, J. D., Prada, F., et al. 2013, ApJ, 770, 77
Fermi-LAT Collaboration 2013, arXiv:1303.2908
Finke, J. D., Razzaque, S., & Dermer, C. D. 2010, ApJ, 712, 238
Franceschini, A., Rodighiero, G., & Vaccari, M. 2008, A&A, 487, 837
Gilmore, R. C. 2012, MNRAS, 420, 800
Gilmore, R. C., Madau, P., Primack, J. R., Somerville, R. S., & Haardt, F. 2009, MNRAS, 399, 1694
Granot, J., Cohen-Tanugi, J., & do Couto e Silva, E. 2008, ApJ, 677, 92
Hascoet, R., Daigne, F., Mochkovitch, R., & Vennin, V. 2012, MNRAS, 421, 525
Kneiske, T. M., Bretz, T., Mannheim, K., & Hartmann, D. H. 2004, A&A, 413, 807
Kneiske, T. M., Mannheim, K., & Hartmann, D. H. 2002, A&A, 386, 1
Kumar, P., Hernández, R. A., Bošnjak, Ž., & Barniol Duran, R. 2012, MNRAS, 427, L40
Primack, J. R., Bullock, J. S., & Somerville, R. S. 2005, in AIP Conf. Proc. 745, High Energy Gamma-Ray Astronomy, ed. F. A. Aharonian, H. J. Völk, & D. Horns (Melville, NY: AIP), 23
Razzaque, S., Dermer, C. D., & Finke, J. D. 2009, ApJ, 697, 483
Salamon, M. H., & Stecker, F. W. 1998, ApJ, 493, 547
Stecker, F. W., Malkan, M. A., & Scully, S. T. 2006, ApJ, 648, 774
Stecker, F. W., Malkan, M. A., & Scully, S. T. 2012, ApJ, 761, 128